

Local Spectral Inversion and Bosonic Fine Structure Extraction via Superconducting Scanning Tunneling Spectroscopy

F. C. Niestemski,^{1,2,*} S. Johnston,^{1,3,*} A. W. Contryman,^{1,4}
C. D. Camp,^{1,2} T. P. Devereaux,^{1,5} and H. C. Manoharan^{1,2,5,†}

¹*Stanford Institute for Materials and Energy Sciences,*

SLAC National Accelerator Laboratory, Menlo Park, California 94025, USA

²*Department of Physics, Stanford University, Stanford, California 94305, USA*

³*Institute for Theoretical Solid State Physics, IFW Dresden,*
Helmholtzstrasse 20, 01069 Dresden, Germany

⁴*Department of Applied Physics, Stanford University, Stanford, California 94305, USA*

⁵*Geballe Laboratory for Advanced Materials,*
Stanford University, Stanford, California 94305, USA

Abstract

We perform the scanning tunneling spectroscopy based superconductor-vacuum-superconductor analogue to the seminal McMillan and Rowell superconductor-insulator-superconductor device study of phonons in the archetypal elemental superconductor Pb [W. L. McMillan and J. M. Rowell, Phys. Rev. Lett. **14**, 108 (1965)]. We invert this spectroscopic data utilizing strong-coupling Eliashberg theory to obtain a local $\alpha^2F(\omega)$ and find broad underlying agreement with the pioneering results, highlighted by previously unobserved electron-hole asymmetries and new fine structure which we discuss in terms of both conventional and unconventional superconducting bosonics.

PACS numbers: 74.55.+v, 74.25.Kc, 74.45.+c, 74.78.-w

It has been well established that the Cooper pairs of conventional superconductors are bound by a “pairing glue” mediated by phonons [1, 2]. The verification of phonon-mediated pairing was facilitated by a combination of experimental evidence including an isotope effect study on elemental Hg [3], tunneling studies on Pb devices by McMillan and Rowell (M&R) and Giaever *et al.* [1, 4], and phonon measurements on Pb by Brockhouse *et al.* [5]. Since tunneling studies played such a crucial role in the original identification of the pairing glue, point contact and device tunneling methods have been in continual employment to study the bosonic structure of both conventional and unconventional superconductors alike [6–8]. Additionally, with recent technological improvements in scanning tunneling spectroscopy (STS) experiments, bosonic information has been recorded for various high transition temperature (high- T_c) superconducting systems utilizing metallic tips [9–15]. This STS-based setup proves superior to superconductor-insulator-superconductor (S-I-S) device tunneling for its ability to measure spectra at single atomic locations rather than large spatial averages, in addition to STS utilizing the cleaner vacuum barrier over the device’s sandwiched insulator.

Remarkably, despite the increasing prevalence of STS bosonic studies, no control experiment has ever been completed where vacuum-based STS is performed on a known conventional system to measure and fully invert the bosonic substructure, verifying it against the known result. This is especially important since certain details of the tunneling process are still under investigation [16–22]. Though conventional superconductors are better understood than their unconventional counterparts, acquiring high-resolution STS spectra on conventional superconductors is more challenging. This difficulty stems from significantly smaller gap sizes (an order of magnitude) which lead to more stringent requirements on noise minimization for resolution comparable to that of high- T_c systems. (These requirements become even more stringent when recording a higher harmonic of the modulation voltage to acquire d^2I/dV^2). There have been numerous prior results for vacuum STS on conventional superconductors but these results have either ignored the bosonic substructure of the spectra while focusing on in-gap states, or not possessed the required energy resolution and noise levels for clean spectroscopy [23–25]. In light of this, as diagrammed in Fig. 1(a) we studied STS on the archetypal elemental superconductor Pb, employing a superconducting Pb tip for feature sharpness and to construct a true vacuum analogue (S-Vac-S) to the M&R device study (S-I-S) [1]. (The reasons for this specific material choice, as well as the detailed experimental method, can be found in the Supplemental Material [SM]). We believe this to be the first inversion study of the phonon spectrum of a conventional superconductor utilizing

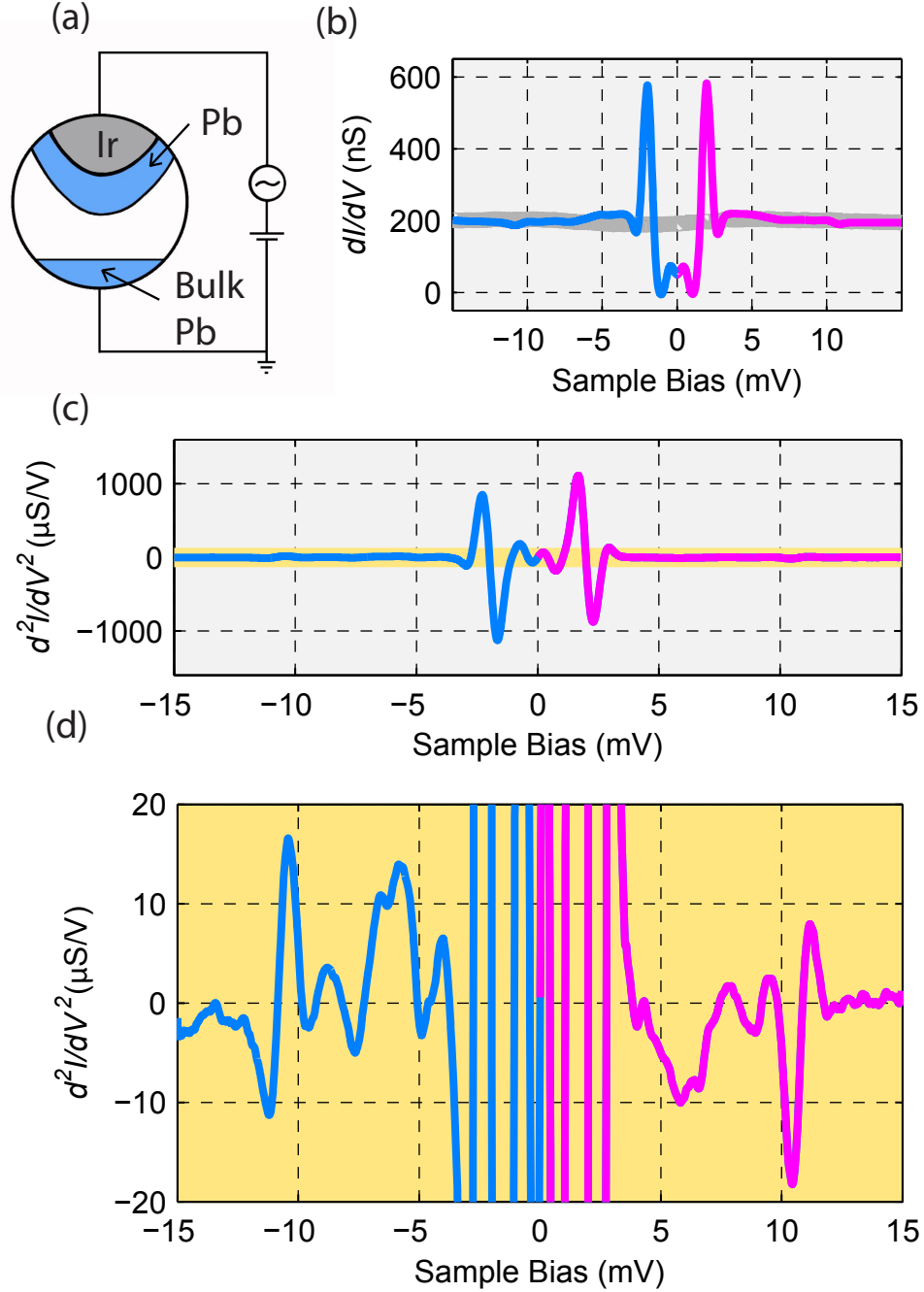


FIG. 1: (a) A diagram of the experimental S-Vac-S setup. (b) Raw dI/dV spectrum at a single location. The negative sample biases, corresponding to occupied electronic states, are colored in blue while the positive biases, corresponding to unoccupied electronic states, are colored in magenta. The spectrum in gray is the normal state spectrum acquired in a magnetic field $B = 1$ T. (c) d^2I/dV^2 by numerical differentiation of the data in (b). The yellow band highlights the range of interest which we zoom in on in (d), showing high-resolution d^2I/dV^2 acquired by HHS.

ultra-high vacuum STS in true tunneling mode.

To verify the superconducting nature of the sample and tip we measured a dI/dV spectrum using the standard lock-in technique [Fig. 1(b)]. The spectrum shows the familiar structure for tunneling between two inequivalent superconductors with tall coherence peaks located at $\Delta = \Delta_{\text{tip}} + \Delta_{\text{sample}}$ ($\Delta_{\text{sample}} > \Delta_{\text{tip}}$) and two in-gap features at $\Delta' = \Delta_{\text{sample}} - \Delta_{\text{tip}}$. From this we obtain $\Delta = 2.0 \pm 0.02$ mV and $\Delta' = 0.42 \pm 0.02$ mV which corresponds to superconducting energy gaps $\Delta_{\text{sample}} = 1.21 \pm 0.02$ mV and $\Delta_{\text{tip}} = 0.79 \pm 0.02$ mV. The Δ_{sample} value agrees well with the expected bulk value and the Δ_{tip} value is consistent with other experimental gap measurements on few-monolayer Pb systems [26, 27].

Continuing outwards from the coherence peaks, sharp dips are observed in dI/dV on both sides of the Fermi energy ε_{F} ($V = 0$) at energy $E_{\text{dip}} = 2.72 \pm 0.02$ mV. This value is equal (within experimental error) to $\Delta_{\text{sample}} + 2\Delta_{\text{tip}}$, but this may be a coincidence. Following the large dips are several step like features that are well known to be associated with electron-boson coupling (phonons, in this case). These features are best analyzed by examining d^2I/dV^2 vs. V [Fig. 1(c)] which can be directly related [1] to the effective electron-boson coupling function $\alpha^2(\omega)$ and the boson density of states $F(\omega)$ for bosons of energy ω . We will discuss the dI/dV dips in detail later in the Letter and first focus on the bosonic features (which are reported in terms of Ω where $\Omega = \omega - \Delta$).

The largest d^2I/dV^2 signal [Fig. 1(c)] comes from the sharpness of the coherence peak which is two orders of magnitude larger than the other peaks. In order to resolve the much weaker signal from the boson substructure it is necessary to tune the settings of the tunnel junction and lock-in preamplifier to zoom in specifically on these higher energy features. To highlight these complex spectral features we utilize a second lock-in preamplifier tuned to twice the modulation frequency to directly resolve d^2I/dV^2 , which we will refer to as higher-harmonic spectroscopy (HHS) [Fig. 1(d)].

In order to compare this data with the M&R device data, the M&R result has been digitized, thermally broadened, and overlaid with this study's result (see [SM]). It can be seen that the STS based S-Vac-S data is in excellent agreement with the M&R device S-I-S study (Fig. 2). The differences between the two sets of data will be highlighted and further analyzed later in the Letter.

Unlike HHS, the M&R method calls for taking dI/dV in the superconducting state, dividing it by dI/dV in the normal state, and differentiating the result. This was necessary in order to divide out any spurious signals resulting from the insulating tunneling barrier which might contribute

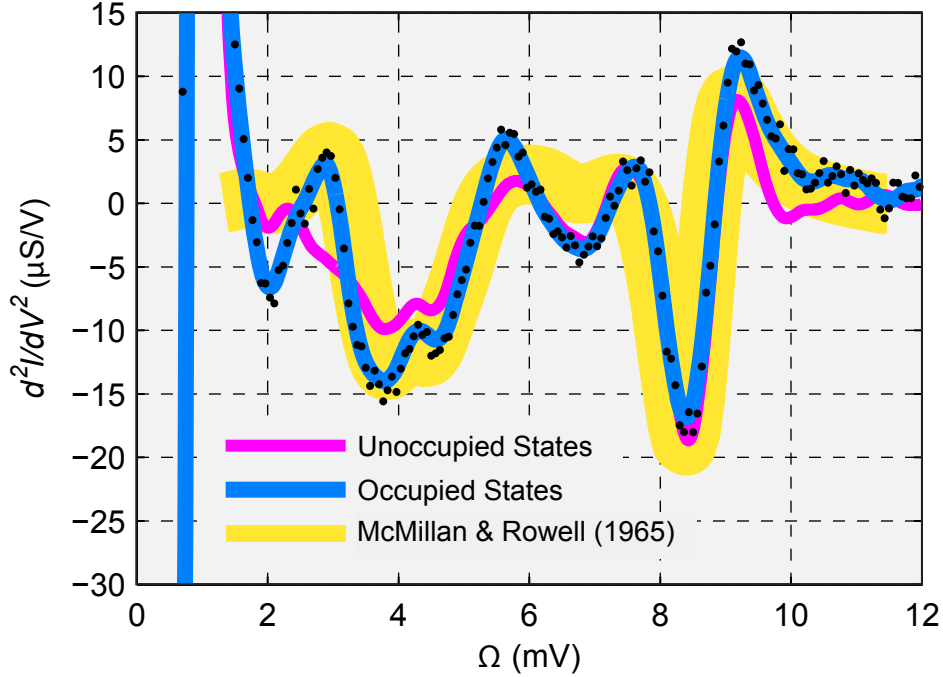


FIG. 2: Smoothed d^2I/dV^2 vs. Ω comparing the occupied and unoccupied spectra from this experiment with the M&R device result [1]. (Occupied curve is $-d^2I/dV^2$). The M&R data has been thermally broadened from the 0.8 K at which the data was recorded to 4.2 K to match this experiment (see [SM]). The occupied electronic states spectrum is accompanied by the raw data (black circles).

inelastically to the tunneling process. Since in our experimental setup the vacuum acts as a perfect insulating barrier, both methods should give similar results. In order to substantiate this claim we repeat this experiment using the traditional M&R method utilizing a 1-T magnetic field (the critical field of Pb is ≈ 0.080 T [28]) and compare the results. It can be seen that the normal state curve is essentially flat when compared to the superconducting state [Fig. 1(b)], so it can be accurately surmised that dividing $dI/dV|_{SC}$ by an approximately flat line will result in essentially the original curve. For thoroughness we nevertheless complete the M&R-prescribed recipe to obtain d^2I/dV^2 using the superconducting and normal state data of Fig. 1(b). The resultant spectra is overlaid on the HHS result in Fig. 3(a). It is evident that the spectra are identical with the exception that the M&R method is much noisier. This verifies that this normal-state division is not necessary for S-Vac-S tunneling in this simple ‘control’ case of tunneling between similar elemental superconductors. This is an important statement for future experiments. Clearly it is experimentally simpler to take one measurement and use raw output rather than to take two

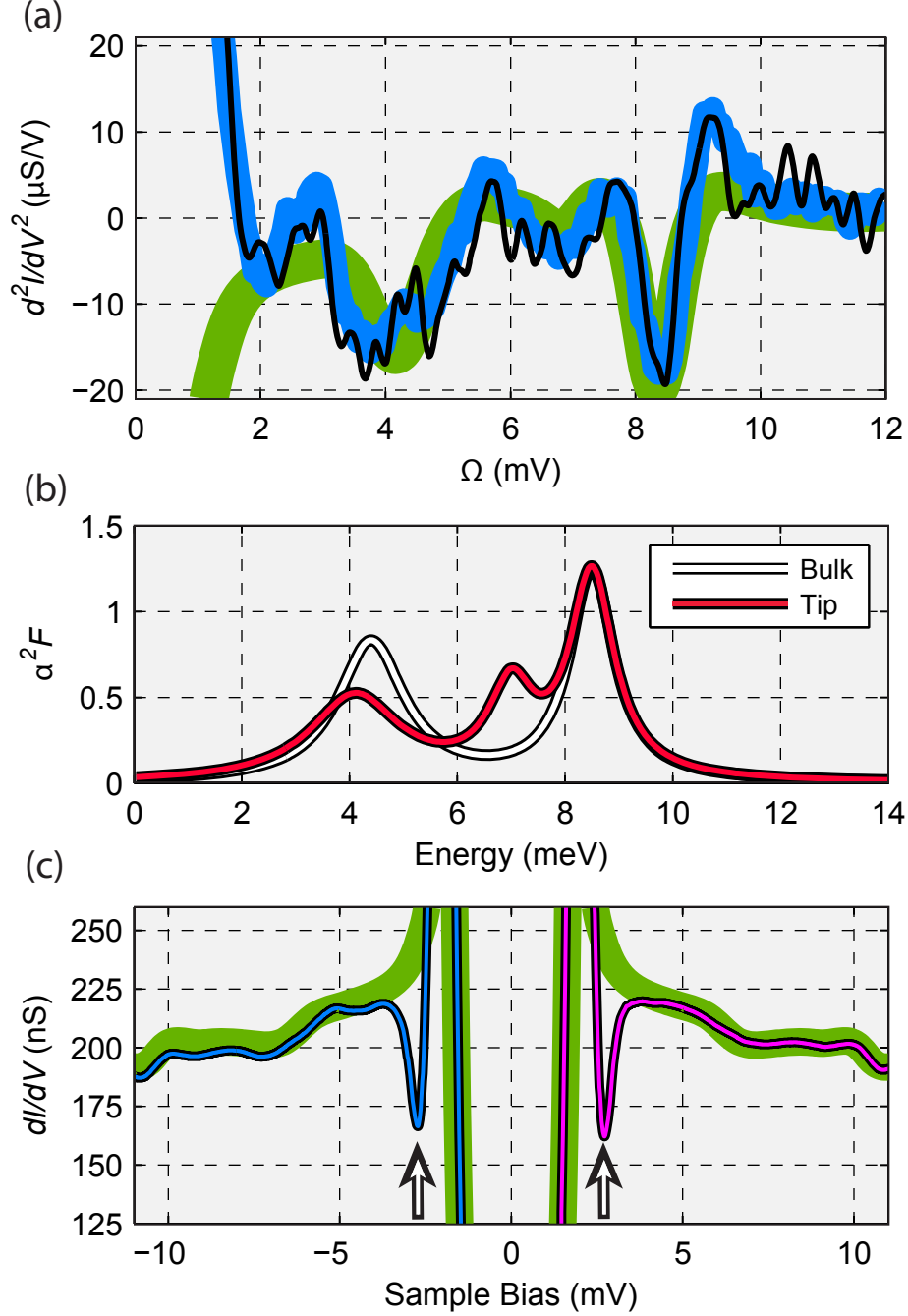


FIG. 3: (a) Comparison of occupied $-d^2I/dV^2$ data by HHS experiment (blue), $-\frac{d}{dV} \left(\frac{dI}{dV} |_{SC} / \frac{dI}{dV} |_N \right)$ experimental data (black), Eliashberg calculation based on model $\alpha^2F(\omega)$ (green). (b) Model $\alpha^2F(\omega)$ altered from the Lorentzian model of Scalapino *et al.* [29]. (c) Experimental dI/dV curve overlaid with Eliashberg-based simulation (green). Note the strong agreement with the exceptions of the large dips symmetric about ϵ_F (white arrows).

measurements at different times, under different conditions, and in combination with a numerical derivative combining the data sets. We have now shown that this efficient single HHS measurement is sufficient. (It is important to note that this is valid since the normal-state spectra is essentially flat. In the specific case of the hole-doped cuprates, where the normal state is highly non-trivial and spatially dependent, such a division might still be necessary [12]).

Since our spectra is so similar to that of M&R it should be straightforward to calculate the tunneling spectra with Eliashberg theory and match it to our experiment. The tunneling current between two superconductors separated by an insulating (or vacuum) barrier is given by $I(V) \propto \int_0^V d\omega N_{\text{SC},1}(\omega) N_{\text{SC},2}(\omega + V) [n_{\text{F}}(\omega) - n_{\text{F}}(\omega + V)]$ where V is the sample bias, $n_{\text{F}}(\omega)$ is the Fermi occupation number, and $N_{\text{SC},1}(\omega)$ and $N_{\text{SC},2}(\omega)$ are the density of states (DOS) for the two respective superconductors. Once $I(V)$ is known, the differential conductance dI/dV and the second derivative d^2I/dV^2 can easily be found numerically. For a strong-coupling superconductor such as Pb, the DOS is given by $N_{\text{SC}}(\omega)/N_{\text{N}}(0) = \text{Re}[\omega/\sqrt{\omega^2 - \Delta^2(\omega)}]$, where the S (N) subscript denotes the superconducting (normal) state, and $N_{\text{N}}(0)$ is the DOS at ϵ_{F} . Here, $\Delta(\omega)$ is the complex frequency-dependent gap function given by the ratio of the anomalous self-energy and the renormalization function $\Delta(\omega) = \phi(\omega)/Z(\omega)$. $Z(\omega)$ and $\phi(\omega)$ are obtained by solving the real-axis Eliashberg equations [29, 30] using $\alpha^2F(\omega)$ as an input and our calculations are therefore dependent on this choice. In this case we have two phonon spectra to consider, one for the bulk sample and one for the tip. For the former we follow Scalapino *et al.* [29] and define α^2F with a sum of Lorentzians (for more details see [SM]). For the latter we modify this model with additional peaks to account for the thin-film nature and geometry of the superconducting tip where coupling can occur with phonon branches normally silent in bulk Pb. Figure 3 shows these model α^2F functions and the resulting dI/dV and d^2I/dV^2 which agree with the experiment (acquired in the two previously described experimental methods). The strongest difference between the two are the strong dips immediately past the coherence peaks in dI/dV [indicated by the arrows in Fig. 3(c)]. These dips are also manifested in d^2I/dV^2 where the curves split at low energies.

The pronounced dips in dI/dV are visually reminiscent of other tunneling studies—for example, break junction tunneling experiments on hole-doped BSCCO-2212 [31] where the authors claim a connection between the spectral dip shapes (often referred to as peak-dip-hump) and bosonic modes. Similar peak-dip-hump structures have been seen numerous times in N-Vac-S standard STS studies on hole-doped BSCCO-2212 as well. Here we make no statement on the origin of these dips in the high- T_c superconductors. We simply note that in our elemental super-

conductor study very similarly shaped dips occur and, in this benchmark case, their absence in $\alpha^2 F(\omega)$ excludes those dips from being relevant to pairing. Similarly shaped dip features have previously been seen in STS S-Vac-S junctions [25, 32, 33], but none of these studies give a compelling explanation for their existence. None of those studies though were able to truly differentiate that dip feature from other bosonic signals as in this work. The most prevalent hypotheses for these features invoke proximity effect where extra features in d^2I/dV^2 are observed in combined S-I-NS junctions [34], surface impurity considerations [32], or k -selective tunneling processes in two-band superconductivity [33]. While a multiband model might not be appropriate for the case of Pb, the underlying idea of the k -selective tunneling might be relevant due to Pb’s anisotropic superconducting gap [35, 36]. In this experiment the direction of anisotropy for the tip might not align with the anisotropic axis of the bulk. This alignment mismatch may relate to the similar dips in the break junction results between superconductors but does not elucidate peak-dip-hump behavior in standard STS studies with a normal metallic tip.

The sandwich configuration of the M&R device necessarily demanded that occupied and unoccupied states be equivalent since the definition of the “sample” electrode and “tip” electrode could always be re-designated due to identical geometry of the two electrodes. In this experiment, the tunneling electrodes are distinguishable allowing us to differentiate between the occupied and unoccupied states of the bulk sample. Due to the very weak particle-hole asymmetry in Pb, theory demands—and our simulations demonstrate—that no differences between the occupied and unoccupied sides should exist. In our measured spectra the two sides are indeed mostly similar, but variations are in fact present. This particle-hole asymmetry does not have an obvious explanation. Immediately, we can discount the notion of this being an artifact of the tip structure. While it is possible for the electronic structure of the tip to add slope information or distort the measured spectrum through convolution, there is no present theory to account for the tip subtly modifying the phonon structure on only one side of ε_F . To explore these differences more thoroughly, both occupied and unoccupied d^2I/dV^2 spectra were fit with Gaussian peaks. Two different fitting schemes were explored. As a starting point in fitting, the individual peak positions were constrained to be identical for both the occupied and unoccupied states. The experimental asymmetry could be captured by either introducing an extra peak at $\Omega = 2.87$ meV in the unoccupied side or by allowing the FWHM of the dual peak structure near 4 meV to have different values for the occupied and unoccupied sides (see data in Fig. 2). Neither of these fits have a physical basis within Eliashberg theory, however—extra phonon structure cannot exist on only one side of ε_F ,

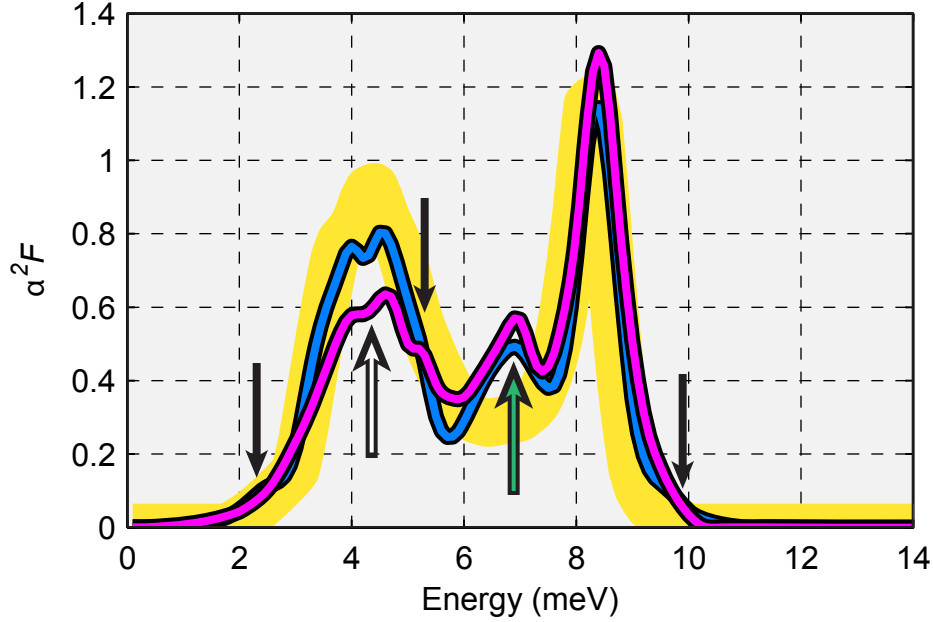


FIG. 4: Calculated $\alpha^2 F(\omega)$ from spectral inversion of d^2I/dV^2 treating the occupied (blue) and unoccupied (magenta) electronic states as separate spectra. The yellow curve is the device $\alpha^2 F(\omega)$ from M&R [1]. Arrows mark features discussed in the text.

nor is there a physical reason for the broadening of the phonon peaks to have different values on alternate sides of ϵ_F . Even more puzzling is the fact that only certain phonon modes seemed to be broadened asymmetrically about ϵ_F while the other modes have broadening symmetric about ϵ_F .

We now advance from the forecasted model of $\alpha^2 F(\omega)$ to a full inversion of the experimental data to calculate $\alpha^2 F(\omega)$. Since the Eliashberg-based inversions are not compatible with occupied/unoccupied asymmetry calculations, this asymmetry can only be explored by treating the occupied and unoccupied sides of the spectra as independent data sets. Another complexity of this calculation is the question of how to treat $\alpha^2 F(\omega)$ in terms of the sample superconductor and tip superconductor. Since the inversion process is based on an iterative process to bring the calculated d^2I/dV^2 progressively closer to the experimental d^2I/dV^2 , leaving both the tip and the sample as separate fitted spectra would result in an infinite number of different solutions to $\alpha^2 F(\omega)$. The most impartial way then to perform the inversion is to constrain the magnitudes of $\alpha^2 F(\omega)_{\text{tip}}$ and $\alpha^2 F(\omega)_{\text{sample}}$ in a fixed ratio determined by their respective Δ values while allowing their linked overall shape to vary. (For a thorough description of the fitting procedure see [SM]).

Fig. 4 shows the inverted $\alpha^2 F(\omega)_{\text{occupied}}$ and $\alpha^2 F(\omega)_{\text{unoccupied}}$ and its general agreement with the M&R result. Using the inverted $\alpha^2 F(\omega)$ spectrum we now have the information necessary to

extract the dimensionless coupling strength $\lambda = \int_0^\infty 2\alpha^2 F(\omega) d\omega / \omega$ from our experimental data. The occupied and unoccupied curves give $\lambda_{\text{occupied}} = 1.38$ and $\lambda_{\text{unoccupied}} = 1.34$ with $\lambda_{\text{average}} = 1.36$ compared to the M&R result of $\lambda_{\text{device}} = 1.33$ [1]. (From a particle-hole symmetric theory it is again unphysical to quote that the coupling strength and thus the T_c is variable for the occupied and unoccupied sides of the spectrum, but from an experimental point of view we have two valid data sets to be used to obtain λ values).

The two strongest differences between this experiment's calculated $\alpha^2 F(\omega)$ and the M&R result are the additional spectral weight around 7 meV (Fig. 4, green arrow) and the splitting of the first peak (Fig. 4, white arrow). These can easily be explained by the thin-film nature of the Pb tip. In a first-principles phonon simulation [37] it was seen that in two-monolayer films the surface lifted the degeneracy of the transverse mode resulting in distinct transverse peaks. It was also seen that increased electron density on the surface resulted in stronger Pb-Pb bonds, stiffening the longitudinal peak which accounts for the added spectral weight seen around 7 meV. (The splitting of the transverse modes can also be explained by enhanced spin-orbit coupling [38], but this option does not explain the weight at 7 meV).

This then takes us to the differences between the occupied and unoccupied inversions of $\alpha^2 F(\omega)$. The black arrows in Fig. 4 highlight these differences. The largest difference is an additional peak in the transverse mode (black arrow near 5 meV). This peak sits roughly in the middle of the range of 3–7 meV in which the occupied and unoccupied spectral data display the most significant contrast (Fig. 2), and is near the 5-meV energy where some shear vertical surface phonons have been measured at energies that have been potentially softened by spin-orbit coupling [39]. This does not offer any explanation as to why this would cause this phonon signal to be different when measured on the occupied vs. unoccupied side. The other difference between the occupied and unoccupied inversions is that $\alpha^2 F(\omega)_{\text{occupied}}$ has two very small peaks, one near 2 meV and one near 10 meV. Since the coupling strength scales inversely with ω , the 2-meV peak is of far greater importance. A peak near this 2 meV energy is also seen both in the occupied and unoccupied spectra of $d^2 I / dV^2$ (although at different strengths). This peak energy is very close to the Kohn anomaly in the transverse acoustic phonon at $q = (0.26, 0.26, 0)$ measured at energy $E = 2.32$ meV recently by inelastic neutron scattering [40]. It had been suggested that such a Kohn anomaly is caused by spin-orbit coupling or many-body interactions and has a correlation to the size of the superconducting gap 2Δ . This correlation though is controversial and may be coincidental [41]. Nothing about the way we understand these anomalies lends a suitable explanation

as to why they would appear stronger or weaker (or not exist at all) in the occupied vs. unoccupied spectra. Theories that include electron-hole asymmetries [42] may need to be considered.

This work was supported by the U.S. Department of Energy, Office of Basic Energy Sciences, Division of Materials Sciences and Engineering, under contract DE-AC02-76SF00515. F. N. acknowledges support from the Karl A. Van Bibber Fellowship and S. J. acknowledges support from the Foundation for Fundamental Research on Matter (FOM, The Netherlands) We thank A. V. Balatsky and M. R. Beasley for discussions and comments.

* These authors contributed equally to this work.

† Electronic address: manoharan@stanford.edu

- [1] W. L. McMillan and J. M. Rowell, *Phys. Rev. Lett.* **14**, 108 (1965).
- [2] J. Bardeen, L. N. Cooper, and J. R. Schrieffer, *Phys. Rev.* **108**, 1175 (1957).
- [3] C. A. Reynolds, B. Serin, W. H. Wright, and L. B. Nesbitt, *Phys. Rev.* **78**, 487 (1950).
- [4] I. Giaever, H. R. Hart, and K. Megerle, *Phys. Rev.* **126**, 941 (1962).
- [5] B. N. Brockhouse, T. Arase, G. Caglioti, K. R. Rao, and A. D. B. Woods, *Phys. Rev.* **128**, 1099 (1962).
- [6] E. L. Wolf, T.-P. Chen, and D. M. Burnell, *Phys. Rev. B* **31**, 6096 (1985).
- [7] Q. Huang, J. F. Zasadzinski, and K. E. Gray, *Phys. Rev. B* **42**, 7953 (1990).
- [8] J. G. Rodrigo, N. Agraït, C. Sirvent, and S. Vieira, *Phys. Rev. B* **50**, 7177 (1994).
- [9] J. Lee *et al.*, *Nature* **442**, 546 (2006).
- [10] F. C. Niestemski *et al.*, *Nature* **450**, 1058 (2007).
- [11] J. Zhao *et al.*, *Nature Physics* **7**, 719 (2011).
- [12] A. N. Pasupathy *et al.*, *Science* **320**, 196 (2008).
- [13] N. Jenkins *et al.*, *Phys. Rev. Lett.* **103**, 227001 (2009).
- [14] Y. Fasano *et al.*, *Phys. Rev. Lett.* **105**, 167005 (2010).
- [15] L. Shan *et al.*, *Phys. Rev. Lett.* **108**, 227002 (2012).
- [16] J. Tersoff and D. R. Hamann, *Phys. Rev. B* **31**, 805 (1985).
- [17] C. J. Chen, *Phys. Rev. B* **42**, 8841 (1990).
- [18] W. Sacks and C. Noguera, *Phys. Rev. B* **43**, 11612 (1991).
- [19] S. Pilgram, T. M. Rice, and M. Sigrist, *Phys. Rev. Lett.* **97**, 117003 (2006).
- [20] J. Nieminen, H. Lin, R. S. Markiewicz, and A. Bansil, *Phys. Rev. Lett.* **102**, 037001 (2009).

- [21] S. Johnston and T. P. Devereaux, Phys. Rev. B **81**, 214512 (2010).
- [22] C. Berthod and T. Giamarchi, Phys. Rev. B **84**, 155414 (2011).
- [23] M. Ternes *et al.*, Phys. Rev. B **74**, 132501 (2006).
- [24] S.-H. Ji *et al.*, Phys. Rev. Lett. **100**, 226801 (2008).
- [25] S. H. Pan, E. W. Hudson, and J. C. Davis, Appl. Phys. Lett. **73** (1998).
- [26] S. Qin, J. Kim, Q. Niu, and C.-K. Shih, Science **324**, 1314 (2009).
- [27] C. Brun *et al.*, Phys. Rev. Lett. **102**, 207002 (2009).
- [28] J. Eisenstein, Rev. Mod. Phys. **26**, 277 (1954).
- [29] D. J. Scalapino, in: *Superconductivity* Vol. 1 (Marcel Dekker, 1969), chap. 10, pp. 449–560.
- [30] J. P. Carbotte, Rev. Mod. Phys. **62**, 1027 (1990).
- [31] Y. DeWilde *et al.*, Phys. Rev. Lett. **80**, 153 (1998).
- [32] K. J. Franke, G. Schulze, and J. I. Pascual, Science **332**, 940 (2011).
- [33] Y. Noat *et al.*, Phys. Rev. B **82**, 014531 (2010).
- [34] E. L. Wolf, J. Zasadzinski, J. W. Osmun, and G. B. Arnold, J. Low Temp. Phys. **40**, 19 (1980).
- [35] P. G. Tomlinson and J. P. Carbotte, Phys. Rev. B **13**, 4738 (1976).
- [36] G. I. Rochlin, Phys. Rev. **153**, 513 (1967).
- [37] J. Noffsinger and M. L. Cohen, Phys. Rev. B **81**, 214519 (2010).
- [38] R. Heid, K.-P. Bohnen, I. Y. Sklyadneva, and E. V. Chulkov, Phys. Rev. B **81**, 174527 (2010).
- [39] I. Y. Sklyadneva, R. Heid, K.-P. Bohnen, P. M. Echenique, and E. V. Chulkov, J. Phys.: Condens. Matter **24**, 104004 (2012).
- [40] P. Aynajian *et al.*, Science **319**, 1509 (2008).
- [41] S. Johnston, A. P. Sorini, B. Moritz, T. P. Devereaux, and D. J. Scalapino, Phys. Rev. B **84**, 174523 (2011).
- [42] J. Hirsch, J. Phys. Chem. Solids **67**, 21 (2006).